Direct AC-AC Converter Based on Odd Symmetrical No-Differential AC Chopper Legs With Unipolar Modulation Strategy

Dongbo Guo, Tianpeng Du, Chuang Liu, *Member, IEEE*, Pinjia Zhang, *Senior Member, IEEE*, Zhongchen Pei, Guanyu Yan, Guowei Cai, Yibo Wang, and Rutian Wang

***Abstract*—This article proposes a single-phase bipolar pulse-width modulation direct ac–ac converter with unipolar modulation strategy. The converter is composed of two odd symmetrical two-level no-differential ac chopper legs, which can work in non-inverting and inverting modes for the utility voltage sag or swell compensation. The number switches working at high frequency in each operating mode are minimized thanks to the proposed unipolar modulation strategy, so the total switching losses can be effectively reduced in theory, and the efficiency of the converter is improved. In addition, capacitor symmetry can be realized in the positive and negative half cycle of the input voltage, and the converter has no commutation problems. Finally, on the basis of theoretical analysis, the experimental results under different working conditions are also provided to verify the correctness of the theoretical analysis and the superiority of the proposed topology and modulation strategy.**

***Index Terms*—Bipolar voltage gain, direct ac–ac converter, odd symmetrical, switching losses, unipolar modulation strategy.**

I. Introduction

RECENTLY, with the popularity of renewable energy sources such as wind power and photovoltaics, the voltage fluctuation in the power grid has been exacerbated [1]. To meet the requirements of sensitive loads for voltage stability [2], ac–ac converters are usually used to improve the power quality and provide a stable ac voltage for the loads. Commonly used ac–ac converters can be divided into three types: indirect converters (ac–dc–ac) [3], [4], [5], [6]; matrix converters [7], [8], [9], [10]; and direct ac–ac converters [11], [12], [13]. For the ac–dc–ac converter, two-stage power conversion is required, the existence of the dc link increases the volume and loss of the converter, reduces the conversion efficiency, increases the maintenance cost. For the matrix converter, although the amplitude and frequency of the voltage can be adjusted at the same time, its circuit structure is complex, and the transmission efficiency and voltage gain are relatively low. The direct PWM ac-ac converter has no dc link and only needs a single power conversion, so the efficiency and power density of the converter can be improved, and it has outstanding advantages when only the voltage amplitude needs to be adjusted.

The buck, buck-boost, and Cuk converters proposed in the literature [14], [15], [16] use fewer switching devices and passive components, which have the advantages of simple structure and high conversion efficiency. However, due to the use of bidirectional switches, during the commutation process switches may experience voltage spikes or current spikes, seriously affecting the reliability of the converter. The switching cell connected in series by MOSFET and diode [17], [18], [19], which solves the commutation problem through additional coupling inductors, but the additional diodes and inductors may increase the loss of the converter. The biggest defect of the above converter [14], [15], [16], [17], [18], [19] is that it can only output unipolar voltage and cannot solve voltage swell and sag at the same time. Therefore, it is necessary to develop a converter that can output bipolar voltage [20], [21], [22], [23], [24], [25], [26], [27], [28], [29], [30]. In [20], [21], and [22], Z-source topology is adopted to obtain wide-range bipolar voltage gain, but the converter suffers from commutation problems due to the use of bidirectional switches [23], [24], [25], [26]. In [20] and [21], a special commutation strategy was applied, but reliable and safe commutation could not be achieved. In [22], an resistor-capacitor-dc-blocking (RCD) absorption circuit was used to suppress the voltage spike on the switch, which not only complicates the circuit structure but also increases the extra loss. In [27] and [28], the proposed topology adopts fewer active switches and passive components, which can not only output bipolar voltage but also has no commutation problem. However, the converter proposed in [27] and [28] has the problem of the input and output having no common ground. In addition, the converter proposed in [27] has an asymmetric bipolar operating mode. To overcome this, a common-ground and noninverting/inverting ac–ac converter was proposed in [29], [30]. This converter can

Manuscript received 11 October 2022; revised 26 February 2023 and 13 May 2023; accepted 16 June 2023. Date of publication 27 June 2023; date of current version 28 July 2023. This work was supported by the National Natural Science Foundation of China (Project Name: Direct AC/AC Hybrid Distribution Transformer and Its Basic Application in Flexible Control of Distribution Network; under Grant 52107182). Recommended for publication by Associate Editor M. Amirabadi. *(Corresponding author: Chuang Liu.)*

Dongbo Guo, Tianpeng Du, Chuang Liu, Zhongchen Pei, Guowei Cai, Yibo Wang, and Rutian Wang are with the Northeast Electric Power University, Jilin 132012, China (e-mail: neepugdb@163.com; dtp15764650347@163.com; victorliuchuang@163.com; neepupeizhongchen@163.com; cai4806439@126.com; 469682939@qq.com; wrtmail@163.com).

Pinjia Zhang is with the Tsinghua University, Beijing 100084, China (e-mail: pinjia.zhang@ieee.org).

Guanyu Yan is with the Beihua University, Jilin City 132013, China (e-mail: guanyu0515@126.com).

Color versions of one or more figures in this article are available at https://doi.org/10.1109/TPEL.2023.3289792.

Digital Object Identifier 10.1109/TPEL.2023.3289792

achieve the common ground between input and output voltages and has continuous input and output. On this basis, although the converters proposed in [31] and [32] only realize the input and output common ground connection under some conditions, it not only overcomes the commutation problems, but also has one advantage of realizing the symmetrical bipolar operating mode. Nevertheless, the converters proposed in [31] and [32] have a common defect that the modulated signals are all high-frequency signals. In the working circuit, more switches are working at high frequency, which increases the switching loss.

The converter proposed in this article has symmetrical bipolar working mode, which can effectively solve the problem of voltage sag and swell. In addition, the converter has no commutation problems, and there is no loss of buffer circuit or special commutation strategy. The most prominent advantage of this article is the proposed modulation strategy, which uses fewer high-frequency modulation signals. Under resistive load, the converter has only one switch operating at high frequency per half-wave and there is no dead time. Under inductive load, there are only two switches operating at high frequency. In addition, the converter uses only one inductor (L_f), which effectively reduces stray resistance losses and core losses. All the above characteristics of the converter are verified on the built 1kW prototype. The rest of this article is organized as follows. The description of the proposed topology and PWM modulation principles are arranged in Section II. Section III investigates the working process of the proposed converter. Section IV presents the design considerations of the key components in the converter. The loss of the converter is calculated theoretically in the Section V. The experimental results illustrating the performance of the converter are presented in Section VI. Finally, Section VII concludes the article.

II. Description of the Proposed Topology and PMW Modulation Principles

A. Topology of the Proposed Converter

The proposed converter consists of two completely odd symmetry two-level nondifferential ac chopper legs, which is different from the converter proposed in [29]. However, similar to the converter mentioned in [29], each ac chopper leg of the proposed converter is also composed of four fully controlled switches (such as IGBT) and one absorption capacitor, as shown in Fig. 1. By adjusting the direction of switches and optimizing its modulation strategy, the number of switches working at high frequency in each operating mode is reduced, the switching loss is reduced theoretically. Another advantage is that input capacitor C_{in} is always connected in parallel with one of the absorption capacitors C_1 or C_2 in any working mode. Therefore, capacitor symmetry is achieved.

The converter adopts eight IGBT, among which $S_1 \sim S_4$ can be selected according to load type and working mode. For resistive loads, the switches S_2 and S_3 can employ diodes instead of full controlled switches when the output voltage of the converter is in phase with the input source voltage, diodes also can be used to replace the full controlled switches S_1 and S_4 when the output voltage of the converter is out of phase with the input source

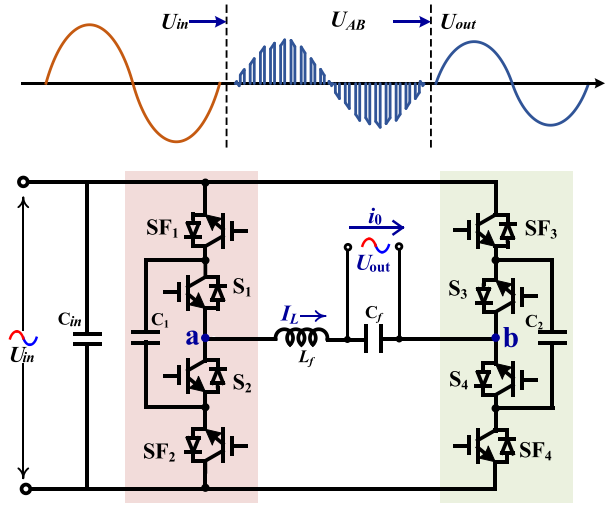

Fig. 1. Schematic of the proposed converter.

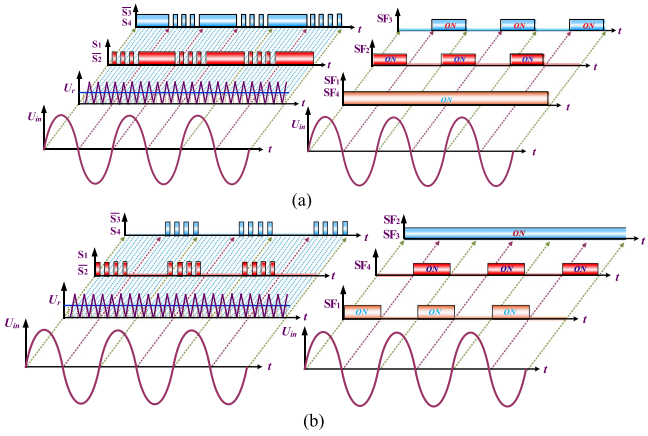

Fig. 2. Unipolar PWM modulation principles. (a) Modulation signal under mode 1. (b) Modulation signal under mode 2.

voltage. At this time, there is only one switch working at high frequency in the positive and negative half cycle of input voltage, which not only simplifies the converter structure but also does not exist dead time. For inductive loads, it needs to be replaced with full controlled switches IGBT.

B. Unipolar Modulation Strategy

The unipolar modulation strategy adopted by the converter proposed in this article is shown in Fig. 2. The biggest advantage of this modulation strategy is that it has fewer high-frequency modulation signals. It can be seen that SF1, SF_2, SF3, and SF_4 always operates at low frequency, so for IGBT, the requirement for switching frequency can be ignored to reduce the conduction voltage drop, thereby reducing the conduction loss.

III. Operation of the Propose d Converter

According to the gain of the converter output voltage, the converter has two working modes, one is that the output voltage and the input voltage are in phase, and the other is that the

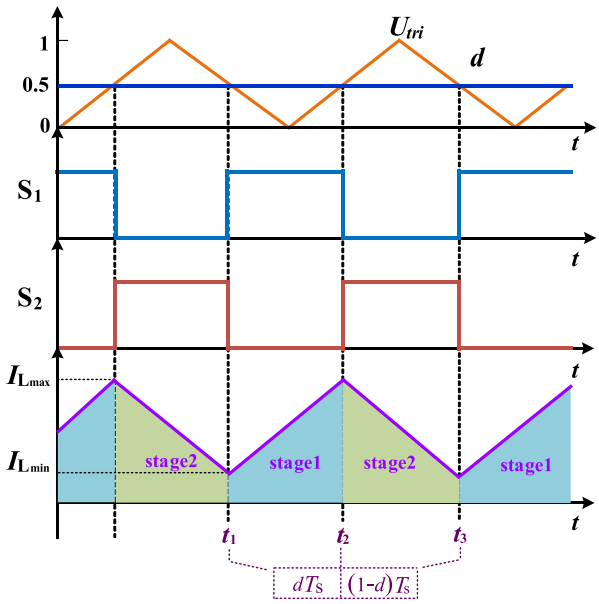

Fig. 3. Modulation signal under mode 1.

output voltage and the input voltage are out of phase. The relationship between the input voltage and the output voltage is shown in formula (1). Where U_{in} is defined as the amplitude of the input line frequency ac voltage (50 Hz), U_{out} is defined as the amplitude of the output line frequency voltage (50 Hz), and d is defined as the time interval when switches are turned on during one switching period. The range of d is from 0 to 1

$$U_{\text{out}} = \pm dU_{\text{in}}. \tag{1}$$

A. Operation Process in Noninverting Mode

In this mode, take positive half wave of input ac voltage as an example to analyze the working process of the converter in detail, the converter has two operating stages, as shown in Fig. 3. When $U_{\text{in}} > 0$, only switches S_1 and S_2 do pulsewidth modulation (PWM) high frequency modulation, the switches SF_1, SF_2, SF_4 and S_4 are in the always on state, and switches S_3 and SF_3 are in the always off state. Additionally, the direction of load current i_0 marked in Fig. 4(a) is defined as positive direction in this article, that is, i_0 is greater than 0 in this direction.

1) *Stage* 1 *[t_1-t_2]:* During [t_1-t_2], S_1 is turned ON, energy of the input ac power is transferred to the load side through the circuit composed of switch SF_1 body diode, S_1, S_4 body diode and SF_4, the working process of the converter can be represented in Fig. 4(a). At this time, the inductor current I_L increases linearly to the maximum value and the converter is in active mode, the input ac power charges input capacitor C_{in} and capacitor C_1, the voltage and current relationship as flows

$$\begin{cases} L_f \frac{dI_L}{dt} = U_{\text{in}} - U_{\text{out}} \\ L_f \frac{(I_{L\text{Max}} - I_{L\text{Min}})}{d \cdot T_{\text{SW}}} = U_{\text{in}} - U_{\text{out}} \end{cases}. \tag{2}$$

2) *Stage* 2 *[t_2-t_3]:* During [t_2-t_3], S_1 is turned OFF and S_2 body diode forward bias, the inductor current I_L forms a closed loop through the load, S_4 body diode, SF_4, SF_2, and D_2. The energy stored on the inductor is released through this loop, so the inductor current linearly decreases as shown in Fig. 3. During this time interval, the converter is in the freewheeling mode (passive mode), and the input capacitor C_{in} and capacitor C_1 are discharged, and the voltage and current relationship as flows

$$\begin{cases} L_f \frac{dI_L}{dt} = -U_{\text{out}} \\ L_f \frac{(I_{L\text{Min}} - I_{L\text{Max}})}{(1-d)T_{\text{SW}}} = -U_{\text{out}} \end{cases}. \tag{3}$$

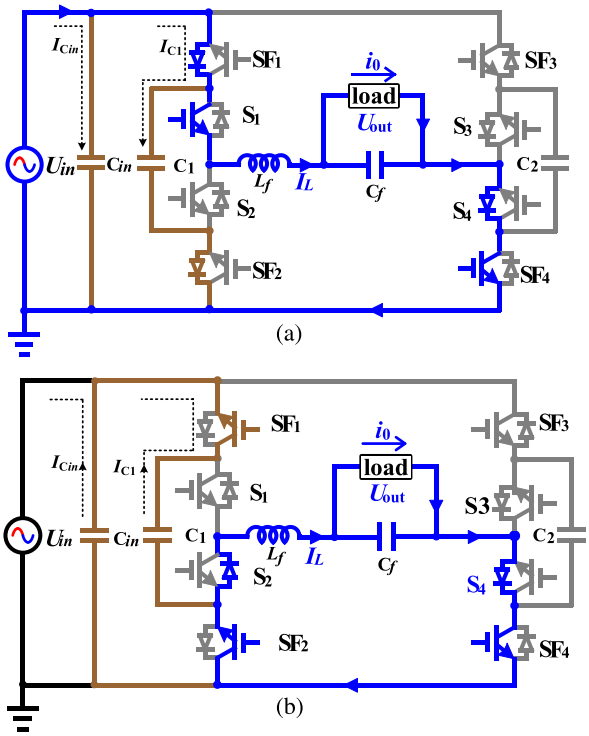

Fig. 4. Two effective switching states of noninverting mode under pure resistive load ($U_{\text{in}} > 0$, $i_0 > 0$). (a) *stage* 1. (b) *Stage* 2.

Based on formula (2) and (3), the relationship between the output voltage and the input voltage is shown in formula

$$U_{\text{out}} = d \cdot U_{\text{in}}. \tag{4}$$

In order to prove that the proposed converter can realize bidirectional energy flow, the operation principle of the converter is analyzed by taking resistive-inductive load as an example. When $U_{\text{out}} > 0$, $i_0 < 0$, if S_1 turns ON and S_2 turns OFF, the current will form a closed loop through S_1 body diode, SF_1, SF_4 body diode, and S_4, as shown in Fig. 5(a); if S_1 turns OFF and S_2 turns ON, current will form a closed loop through S_2, SF_2 body diode, SF_4 body diode, and S_4, as shown in Fig. 5(b). When the power flows forward, the flow path is the same as that under resistive load, so it will not be described. It should be noted that the input capacitor C_{in} and capacitor C_1 are always connected in parallel during the positive half-wave period of input ac voltage, and two capacitors are charged in first half period of the positive half-wave and discharged in second half period of the positive half-wave.

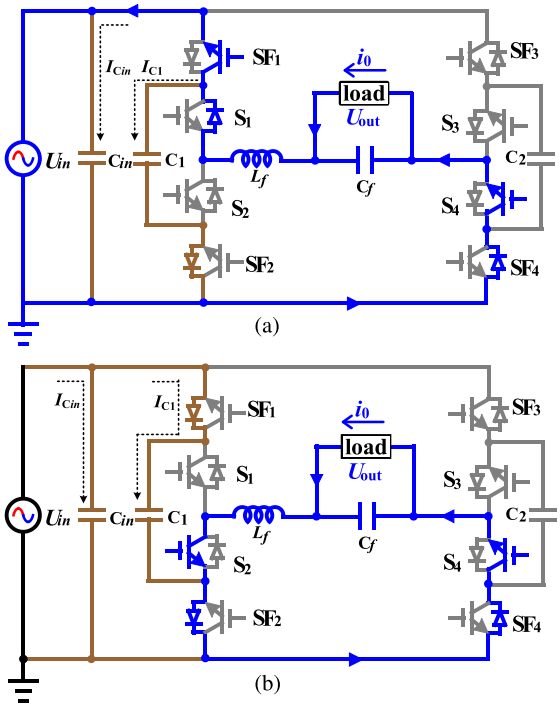

Fig. 5. Two effective switching states of noninverting mode under resistive-inductive load ($U_{\text{in}} > 0$, $i_0 < 0$). (a) *stage* 1. (b) *Stage* 2.

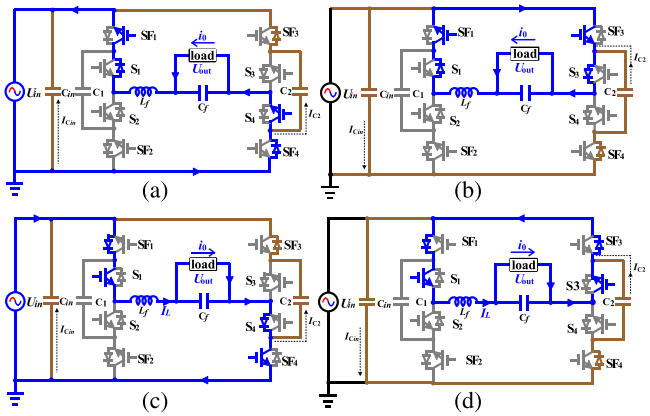

Fig. 6. Working process diagram of converter in noninverting mode when input ac voltage is negative half wave. (a) *Stage* 1 ($U_{\text{in}} < 0$, $i_0 < 0$). (b) *Stage* 2 ($U_{\text{in}} < 0$, $i_0 < 0$). (c) *Stage* 1($U_{\text{in}} < 0$, $i_0 > 0$). (d) *Stage* 2 ($U_{\text{in}} < 0$, $i_0 > 0$).

When input ac voltage is negative half wave, switches S_3 and S_4 do PWM high-frequency modulation, switches S_1, SF_1, SF_3 and SF_4 are always on state, S_2 and SF_3 are always OFF state, and input capacitor C_{in} and capacitor C_2 are in parallel. Besides, the converter works similarly in positive and negative half wave of input ac voltage, which will not be described again in this article. But the article gives working process diagram of the proposed converter when input ac voltage is negative half wave, as shown in Fig. 6.

B. Operation Process in Inverting Mode

In this mode, the converter also has two operating stages shown Fig. 7, and the output voltage of the converter is out

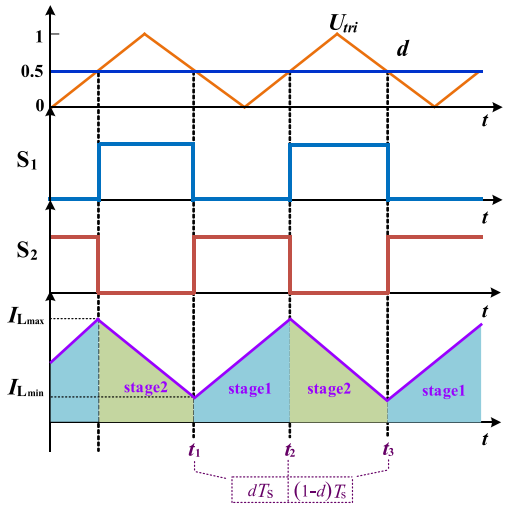

Fig. 7. Modulation signal under mode 2.

of phase with the input voltage. Under resistive load, two diodes can also be used as switches S_1 and S_4. Similar to the analysis when the converter operates in mode 1, the positive half wave of the input voltage is still taken as an example for analysis in mode 2. In this mode, only switch S_2 operating at high frequency, the switches SF_1, SF_2, SF_3, and S_3 are always on, and SF_4, S_4 are always OFF.

1) *Stage* 1 *[t_1-t_2]:* The switch S_2 is on state during this period, the inductor and load are charged from the source through SF_3, S_3 body diode, S_2 and SF_2 body diode. The capacitor C_1 is charged, $U_{C1} = U_{\text{in}}$, and the charging current I_{C1} flows through the body diodes of SF_1 and SF2, and the input capacitor C_{in} is also charged, and the charging current I_{Cin} is shown in the dotted line marked in Fig. 8(a). The input capacitor C_{in} and capacitor C_1 are in parallel during this time interval. The converter is also in active mode (the energy of input ac power is transferred to the load side), and the working process is shown in Fig. 8(a). At this time, the voltage relationship of the working loop is shown in formula

$$\begin{cases} -L_f \frac{dI_L}{dt_1} = U_{\text{in}} + U_{\text{out}} \\ -L_f \frac{(I_{L\text{Max}} - I_{L\text{Min}})}{dT_{\text{SW}}} = U_{\text{in}} + U_{\text{out}} \end{cases}. \tag{5}$$

2) *Stage* 2 *[t_2-t_3]:* When S_2 turns OFF, the energy stored on the inductor is released, the working process is shown in Fig. 8(b). The capacitor C_1 and input capacitor C_{in} are discharged in this time interval, $U_{C1} = U_{\text{in}}$, $U_{C\text{in}} = U_{\text{in}}$, and the discharge current $I_{C\text{in}}$ and I_{C1} of two capacitors (C_{in}, C_1) are, respectively, marked in Fig. 8(b). The input capacitor C_{in} and capacitor C_1 are also in parallel during this time interval. The voltage relationship of the working loop is shown in formula

$$\begin{cases} L_f \frac{dI_L}{dt_2} = -U_{\text{out}} \\ -L_f \frac{(I_{L\text{Min}} - I_{L\text{Max}})}{(1-d)\cdot T_{\text{SW}}} = -U_{\text{out}} \end{cases}. \tag{6}$$

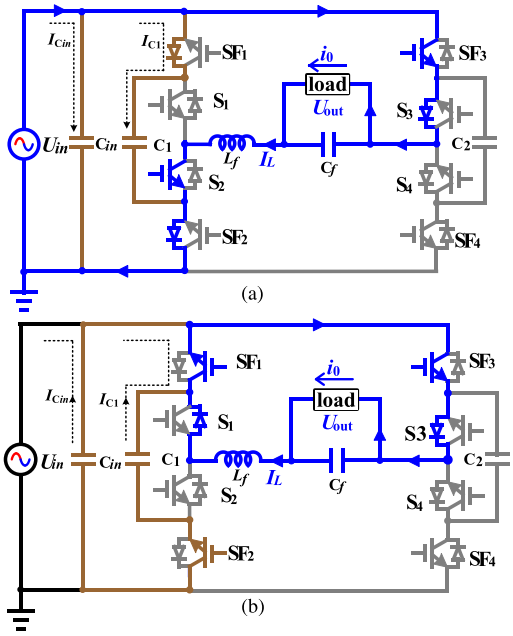

Fig. 8. Two effective switching states of inverting mode under pure resistive load ($U_{\rm in} > 0$, $i_0 < 0$). (a) *Stage* 1. (b) *Stage* 2.

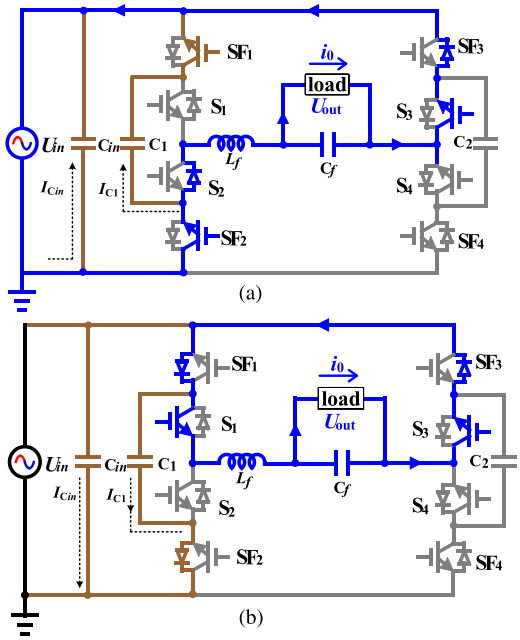

Fig. 9. Two effective switching states of inverting mode under resistive-inductive load ($U_{\rm in} > 0$, $i_0 > 0$). (a) *Stage* 1. (b) *Stage* 2.

Based on formula (5) and formula (6), the relationship between the output voltage and the input voltage is shown in formula

$$U_{\rm out} = -d \cdot U_{\rm in}. \tag{7}$$

Like mode 1, take resistive-inductive load as an example to analyze the operation process of converter in inverting mode. When $U_{\rm in} > 0$, $i_0 > 0$, if S_2 turns ON and S_1 turns OFF, the converter is also in active mode, the energy at power supply side is transferred to load side through switch $\rm SF_2$ and body diodes of switches S_2, $S_{3,1}$ and $\rm SF_3$, and the working circuit is shown in Fig. 9(a); If S_2 turns OFF and S_1 turns ON, the converter is in freewheeling mode. In this mode, the energy of power supply cannot be transferred to load side, and this energy only charges input capacitor $C_{\rm in}$ and capacitor C_1. The working process of the converter during this period can be described in Fig. 9(b). The relationship between voltage-current under resistive-inductive load is the same as that under pure resistive condition, and will not be described again.

When $U_{\rm in} < 0$, the analysis method is the same as when $U_{\rm in} > 0$. To avoid repetition, the analysis is no longer carried out., and similar to noninverting mode, Fig. 10 shows working process of the converter when input ac voltage is negative half wave.

It can be seen from the above analysis that no matter under resistive load or inductive load, the current loop always exists, so there is no commutation problem in the converter. Moreover, the converter has the ability to output bipolar voltage, which can simultaneously address the problem of voltage sag and swell in the power grid.

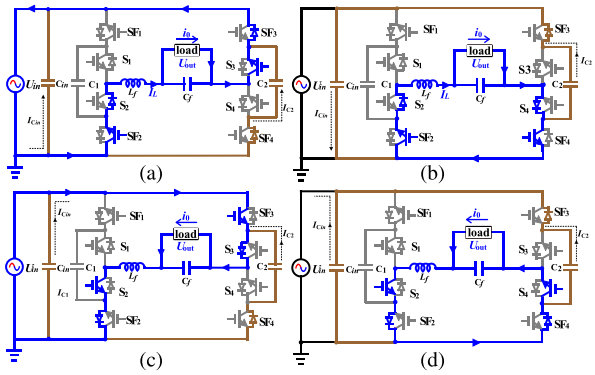

Fig. 10. Working process diagram of converter in inverting mode when input AC voltage is negative half wave. (a) *Stage* 1 ($U_{\rm in} < 0$, $i_0 > 0$). (b) *Stage* 2 ($U_{\rm in} < 0$, $i_0 > 0$). (c) *Stage* 1 ($U_{\rm in} < 0$, $i_0 < 0$). (d) *Stage* 2 ($U_{\rm in} < 0$, $i_0 < 0$).

IV. Design Considerations of Key Components of Converter

Based on the above analysis, the selection guidelines of the proposed converter's key parameters are provided using a scale-down case study in following procedure.

The known parameters: input ac voltage $U_{\rm in}$ is [100–220] Vrms (50 Hz), and converter output voltage gain range is [−1, 1], and maximum output ac voltage is 150 Vrms, and the rated power of the converter prototype is 1 kW. Additionally, assuming that allowable current and voltage ripples $k_i \leq 20\%$ of i_L and $k_u \leq 10\%$ of $U_{\rm out}$ (or $U_{\rm in}$), and the minimum conversion efficiency of the proposed converter is 80%.

A. Selection of Power Switches

The two important bases for selecting the power switches are the maximum current through the switches and the maximum voltage stress. In proposed converter, the maximum voltage stress borne by the power switches is equal to the peak voltage of the input ac voltage, that is, $U_{\text{in.peak}} = 311V$. The maximum current stress of power switches is given by the following equation:

$$I_{\text{max.str.}} = \frac{P_0}{U_{\text{in.min}}\eta_{\min}} = \frac{1000}{100 \times 0.8} = 12.50A \tag{8}$$

Combined with the existing devices in the laboratory, the switches adopted in proposed converter is finally selected as an IKW75N60T IGBT. Although higher switching frequency can effectively decrease volume of output filter, it can be seen from formula (25) that switching frequency is proportional to converter loss. At the same time, based on the reference IKW75N60T date sheet, the frequency of power switch tube is selected as 10 kHz.

B. Design of Output Filter Inductors

Under the two operating modes, the output filter inductor has only two working states in each switching cycle: active state and freewheeling state (passive state). In order to ensure that the converter always works in CCM (current continuous mode), it is necessary to ensure the $I_{L\min} > 0$ under the freewheeling state. According to the principle of conservation, the minimum energy $W_{L.\min}$ released by the inductor in the freewheeling state is equal to the energy $W_{\text{load.max}}$ consumed by the load

$$\begin{cases} W_{L.\min} = \frac{1}{2}L_{\min}(I_{L.\max} - I_{L.\min})^2 \\ \qquad\quad = \frac{1}{2}L_{\min}\left(k_i \cdot \frac{U_{\text{out}}}{Z_{\max}}\right)^2 \\ W_{\text{load.max}} = \frac{U_{out}^2}{Z_{\min}}(1 - d_{\min}) \cdot \frac{1}{f_S} \end{cases}. \tag{9}$$

In order to ensure that the current of converter is continuous in the continuous current state, formula (9) needs to meet the following relationship:

$$W_{L.\min} \geq W_{\text{load.max}}. \tag{10}$$

The simultaneous formula (9) and (10) can get the formula

$$L_{\min} \geq \frac{2Z_{\max}^2}{k_i^2 \cdot Z_{\min}} \cdot (1 - d_{\min}) \cdot \frac{1}{f_S}. \tag{11}$$

The minimum value of output filter inductance is 0.369 mH by bringing specific parameters into (11). Considering the existing inductance in the laboratory and saturation characteristics of inductance, the inductance with the inductive value of 0.5 mH is finally selected.

C. Design of Capacitors

1) Design of the Output Filter Capacitor: In order to ensure the quality of the output waveforms, an output filter capacitor is designed to limit voltage ripple. In a switching cycle, when the converter works in the freewheeling state, the filter capacitor C_f discharges and the discharge current of the filter capacitor is equal to the load current. To ensure that the output voltage ripple does not exceed the specified value, the output filter capacitor shall meet the formula (12) based on maximum voltage ripple k_u

$$C_f \geq \frac{i_{0\max}(1 - d_{\max})}{k_u f_s U_{\text{out}}}. \tag{12}$$

In the above formula, i0max is the maximum current of the load, and the value is 7.5 A; $d_{\max}$ is the maximum duty cycle, which is 0.85 in this system. The specific parameter value is brought into formula (12) for calculation. Through calculation, the output filter capacitor value is 7.5 μF, so the CFR box ac-Filter with capacitance value of 10 μF and withstand voltage of 400 Vac is finally selected.

2) Design of Input Capacitor C_{in} and Absorption Capacitor C_1, C_2: From analysis of the operation process of the converter in Section III, it can be seen that whether the converter works in the noninverting mode or inverting mode, the connection relationship between the input capacitor C_{in} and the absorption capacitors C_1 and C_2 is either the input capacitor C_{in} and the absorption capacitors C_1 in parallel or the input capacitor C_{in} and the absorption capacitors C_2 in parallel. In order to ensure that the two parallel capacitors have better current-sharing characteristics, the input and absorption capacitors are designed with the same capacitance value, that is, $C_{\text{in}} = C_1 = C_2 = C$. Similar to formula (12), formula (13) is obtained on the basis of considering the requirements of input voltage ripple

$$2C \geq \frac{i_{\text{in.max}}(1 - d)}{k_u f_S U_{\text{in}}}. \tag{13}$$

Although the larger the capacitance of the input capacitor, the smaller the total distortion rate of the input current, the capacitance value cannot be too large, otherwise the power factor at the input side will be small. Therefore, in order to meet the requirements of input power factor, the capacitance also needs to meet the formula

$$\frac{8CU_{\text{in}}}{T_{l.F}} \leq i_{\text{in}} \cdot \sqrt{1 - \cos\varphi^2}. \tag{14}$$

In formula (14), $T_{l.F}$ represents the period of line frequency input ac voltage, and $\cos\varphi$ represents the input power factor.

In this system, set the input power factor as 0.95 and the input ac voltage frequency as 50 Hz, and bring the parameters into formulas (13) and (14) to obtain the capacitance range of 15.625–44.318 μF. Combined with the existing experimental devices in the laboratory, the input capacitor and absorption capacitor are finally selected as the ac thin film capacitor with a capacitance of 20 μF.

Based on the above analysis, the electrical specifications of the prototype converter are given in Table I.

V. Converter Loss Theoretical Analysis

The converter power loss mainly includes IGBT loss and stray resistance loss. IGBT loss includes conduction loss and switching loss. Based on the IGBT datasheet, the function relation between power loss and junction temperature, voltage, current, and other parameters are obtained by the numerical fitting method, and then IGBT loss is analyzed and calculated.

TABLE I
EXPERIMENTAL PARAMETERS

Parameters	Values
Input voltage U_{in}	[120-220 Vrms]/50 Hz
Output power P_O	1 kW
Output voltage U_{out}	150 Vrms
Switching frequency f_S	10 kHz
Inductance L_f	0.5 mH
Output capacitor C_f	10 μF
Capacitors C_{in}, C_1, C_2	20 μF
Output load {R, R&L}	{20 Ω, 20 Ω and 25 m}

A. Theoretical Calculation of Conduction Loss

The conduction loss can be calculated according to the formula

$$P_S = \frac{1}{T}\int_0^T V_{CE} I_C dt. \tag{15}$$

After linear fitting of IGBT output characteristic curve, the relationship between on-state voltage drop (V_{CE}) and collector current (I_C) can be expressed as follows:

$$V_{CE} = V_{CEO} + I_C R_{CE}. \tag{16}$$

Where V_{CEO} is the threshold voltage of IGBT after linear fitting, R_{CE} is the forward ON-resistance of IGBT after linear fitting. These two fitting parameters are affected by temperature change, which can be expressed as follows:

$$\begin{cases} V_{CEO} = V_{CEO\_25\,^\circ\mathrm{C}} + K_{V_T}(T_J - 25\,^\circ\mathrm{C}) \\ R_{CE} = R_{CE\_25\,^\circ\mathrm{C}} + K_R(T_J - 25\,^\circ\mathrm{C}) \end{cases} \tag{17}$$

where K_{VT} and K_R are the junction temperature coefficients of ON-resistance and threshold voltage, respectively, and T_J represents the actual junction temperature. Based on the formulas (15)–(17), The conduction loss can be expressed as follows:

$$P_S = V_{CEO} I_{C\mathrm{avg}} + R_{CE} I^2_{C\mathrm{rms}} \tag{18}$$

where $I_{C\mathrm{avg}}$ represents the average value of collector current and $I_{C\mathrm{rms}}$ represents the effective value of collector current. The calculation process of diode conduction loss is similar to that of IGBT, and its conduction loss can be expressed as the formula (19). The total conduction loss is shown in formula (20)

$$P_F = V_{FO} I_{F\mathrm{avg}} + R_F I^2_{F\mathrm{rms}} \tag{19}$$

$$P_Z = P_F + P_S. \tag{20}$$

B. Theoretical Calculation of Switching Loss

The IGBT switching process is affected by many factors, such as gate resistor and junction temperature. The switching loss provided in the datasheet is tested under rated conditions, so it can not be used directly. It should be corrected according to the actual working conditions. The energy loss of IGBT in one switching cycle is shown in formula

$$E_{ts} = E^*_{ts\_i_c} \cdot K_{T_j} \cdot K_{R_G} \cdot K_{V_{CE}}. \tag{21}$$

The E_{ts} includes IGBT switching loss and diode reverse recovery loss, and $E^*{}_{ts\_ic}$ is the corresponding energy loss under different collector current. The values of junction temperature influence coefficient (K_{TJ}), voltage influence coefficient (K_{VCE}), and grid resistance influence coefficient (K_{RG}) are shown in formula

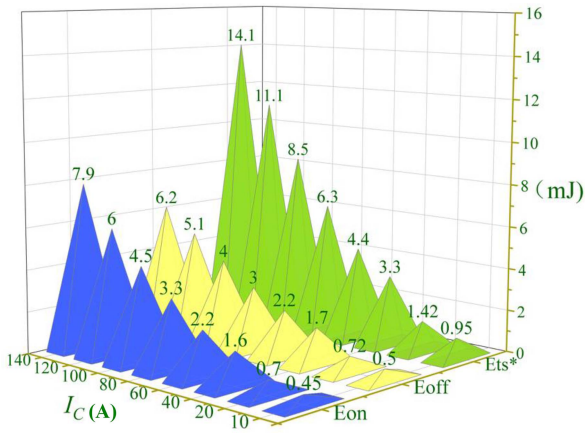

Fig. 11. Switching energy loss as a function of collector current (V_{GE} = 0/15 V, T_J = 175 °C, R_G = 5 Ω, and V_{CE} = 400 V).

$$\begin{cases} K_{V_{CE}} = \left(\frac{V_{CE\_\mathrm{real}}}{V_{CE\_\mathrm{ref}}}\right)^{N_{Tr\_V_{CE}}} \\ K_{T_j} = [1 - N_{T_J}(T_{J\_\mathrm{ref}} - T_{J\_\mathrm{real}})] \\ K_{R_G} = \left(\frac{R_{G\_\mathrm{real}}}{R_{G\_\mathrm{ref}}}\right)^{N_{Tr\_R_G}} \end{cases} \tag{22}$$

where T_{J_ref}, V_{CE_ref}, and R_{G_ref} are junction temperature, collector-emitter voltage, and gate resistor under test conditions respectively; the T_{J_real}, V_{CE_real}, and R_{G_real} are junction temperature, collector emitter voltage, and gate resistor in the actual circuit respectively.

The values of N_{TJ}, N_{Tr_VCE}, and N_{Tr_RG} are obtained by numerical fitting the E_{ts}-T_j, E_{ts}-V_{CE}, and E_{ts}-R_G curves in the datasheet, respectively. Assuming that the switching frequency is f_s, the switching loss power can be expressed as follows:

$$P_{ts} = f_s \cdot E^*_{ts\_i_c} \left(\frac{V_{CE\_\mathrm{real}}}{V_{CE\_\mathrm{ref}}}\right)^{N_{Tr\_V_{CE}}} \cdot \left(\frac{R_{G\_\mathrm{real}}}{R_{G\_\mathrm{ref}}}\right)^{N_{Tr\_R_G}} \cdot [1 - N_{T_J}(T_{J\_ref} - T_J)] \tag{23}$$

Similarly, the turn-ON loss is shown in formula

$$P_{\mathrm{ON}} = f_s \cdot E^*_{\mathrm{on}\_i_c} \left(\frac{V_{CE\_\mathrm{real}}}{V_{CE\_\mathrm{ref}}}\right)^{N_{Tr\_V_{CE\_on}}} \cdot \left(\frac{R_{G\_\mathrm{real}}}{R_{G\_\mathrm{ref}}}\right)^{N_{Tr\_R_{G\_\mathrm{on}}}} \cdot [1 - N_{T_J}(T_{J\_\mathrm{ref\_on}} - T_J)]. \tag{24}$$

The turn-OFF loss is shown in formula (22)

$$P_{\mathrm{OFF}} = f_s \cdot E^*_{\mathrm{off}\_i_c} \left(\frac{V_{CE\_\mathrm{real}}}{V_{CE\_\mathrm{ref}}}\right)^{N_{Tr\_V_{CE\_off}}} \cdot \left(\frac{R_{G\_\mathrm{real}}}{R_{G\_\mathrm{ref}}}\right)^{N_{Tr\_R_{G\_\mathrm{off}}}} \cdot [1 - N_{T_J}(T_{J\_\mathrm{ref\_off}} - T_J)]. \tag{25}$$

Fig. 11 shows the switching loss corresponding to different collector currents under rated conditions provided in the datasheet. The Eon includes turn-on loss and diode reverse recovery loss, Eoff is the turn-OFF loss, and Ets∗ is the total switching loss.

TABLE II
PARAMETERS FOR LOSS ANALYSIS

Parameter	Value
IGBT	IKW75N60T
f_s	10 kHz
$V_{CEO\_25°C}$, $R_{CE\_25°C}$ (I_C<15A)	0.6 V, 20 mΩ
$V_{CEO\_25°C}$, $R_{CE\_25°C}$ (I_C>15A)	0.75 V, 8 mΩ
K_{VT}, K_R	-0.001, 0.05
$V_{FO\_25°C}$, $R_{F\_25°C}$ (I_C<15A)	0.65 V, 22 mΩ
V_{CE_ref}, R_{G_ref}, T_{J_ref}	400 V, 5 Ω, 75 °C
N_{Tr_VCE}, N_{Tr_RG}, N_{TJ}	1.6, 0.46, 0.00162
ESR of capacitor C_f	2.5 mΩ
Parasitic resistances of L_f	140 mΩ

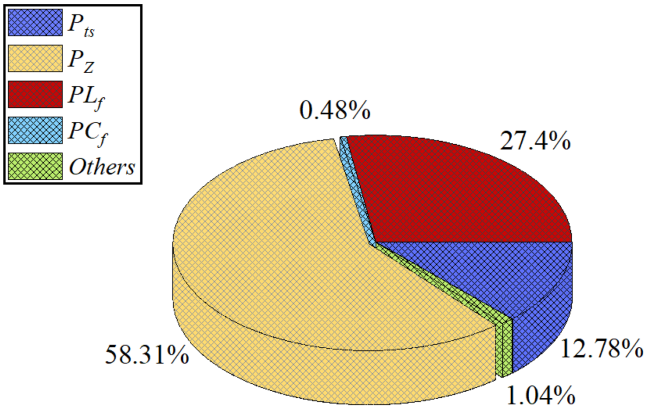

Fig. 12

Fig. 12. Loss distribution of the proposed converter.

C. Converter Power Loss Distribution

In order to determine the various losses of the proposed converter, the parameters for loss analysis are given in Table II. The operating conditions assume that $U_{\text{in}} = 200$ Vrms, $U_{\text{out}} = 150$ Vrms, $P_o = 1000$ W, $f_s = 10$ kHz, and $T_J = 75$ °C. PSIM software can be used to measure the collector-emitter voltage (V_{CE}) and the collector current (I_C) of the switch, and then the conduction loss can be calculated through formulas (15)–(20). Combining formula (23), Table II and Fig. 11, the switching loss can be calculated.

The loss distribution of the proposed converter is presented in Fig. 12. It can be seen that approximately 59% of the power loss comes from conduction loss, this is because IGBTs have fixed threshold voltage (V_{CEO}) and most of the switches in the working loop are always on.

VI. Analysis Of Experimental Results

A. Prototype

To validate the rationality of the proposed converter, a 1 kW prototype is built for testing based on theoretical analysis and simulation verification, shown in Fig. 13. The prototype was tested in two working modes, including resistive load and resistive-inductive load. The specific experimental parameters are given in Table I.

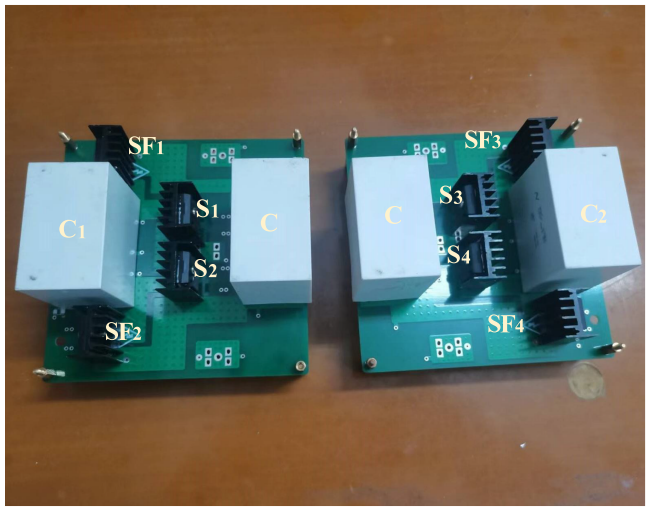

Fig. 13. Photograph of experimental prototype.

B. Experimental Results of Converter Under Different Working Conditions

Fig. 14 shows the results of the converter under operating noninverting mode when the load is pure resistive load, the input voltage is 200 Vrms, and the output voltage is 150 Vrms. The partial signal waveforms of the switches are shown in Fig. 14(a). It can be seen that only one switch operates at high frequency. Fig. 14(b) shows the waveforms of input voltage, output voltage and output current, which are highly sinusoidal, and there is almost no phase shift between the output voltage and the output current. Fig. 14(c) shows the high-frequency voltage before filtering (U_{ab}) and the output filter inductor current (I_L). It can be seen from the partial enlarged detail that there are two change processes in the inductor current. When S_1 turns ON, the inductor and load are charged from the source, and the voltage before filtering (U_{ab}) is equal to the input voltage (U_{in}). When S_1 turns off, the inductor will be freewheeling, and the voltage before filtering (U_{ab}) is approximately equal to zero. The experimental results are consistent with theoretical analysis.

Fig. 15 shows the results waveforms of the converter under operating mode 1 when the load is resistive-inductive load. Fig. 15(a) shows the switches signal waveforms. To prevent the short circuit of the bridge arm, the dead time of the 2 μs is set between S_1 and S_2. Fig. 15(b) shows the waveforms of input voltage, output voltage, and output current under resistive-inductive loads condition. It can be seen that there is an obvious phase offset between the output voltage (U_{out}) and the output current (i_0), which verifies that the converter can realize bidirectional power flow.

Fig. 16 shows the results waveforms of the converter under operating inverting mode when the load is pure resistive load. Fig. 16(a) shows the waveforms of input voltage (U_{in}), output

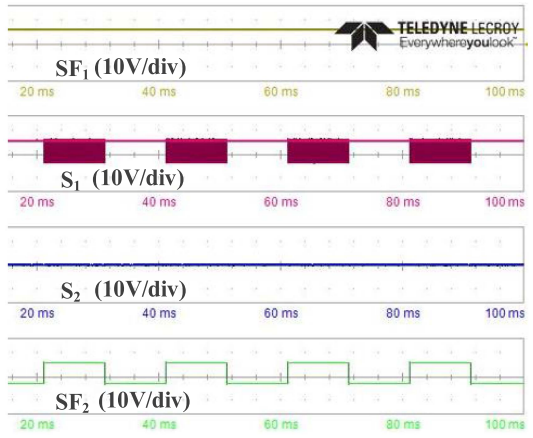

(a)

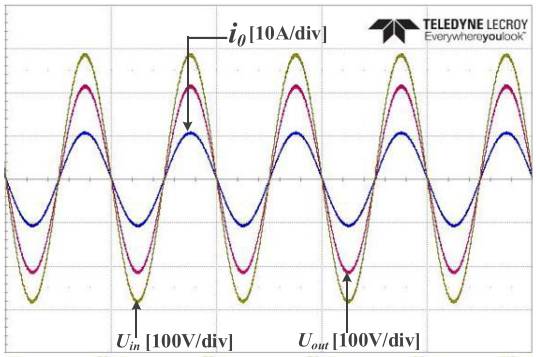

(b)

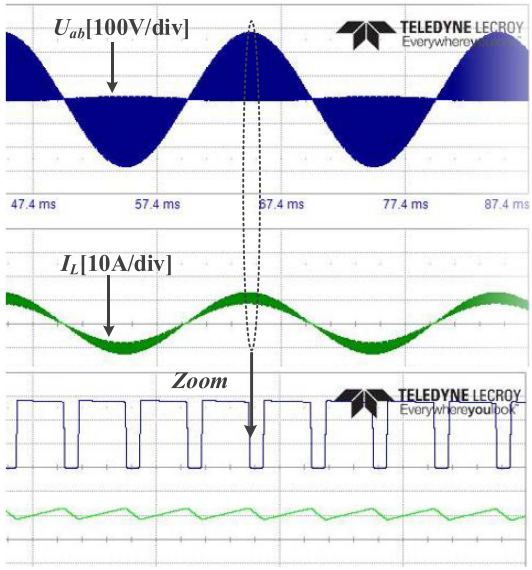

(c)

Fig. 14. Experimental waveformss of mode1 under resistive load ($U_{\text{in}} = 200$ Vrms, $U_{\text{out}} = 150$ Vrms, and $R = 20\ \Omega$).

voltage (U_{out}), output filter inductor current (I_L), and output current (i_0). As can be seen from Fig. 16(a), U_{in} and U_{out} are out of phase, that is, their phases are 180° different from each other. I_L is always higher than zero, so the converter operates in CCM. Similar to mode 1, the inductor current (I_L) also has two changes processes in inverting mode. The voltage across

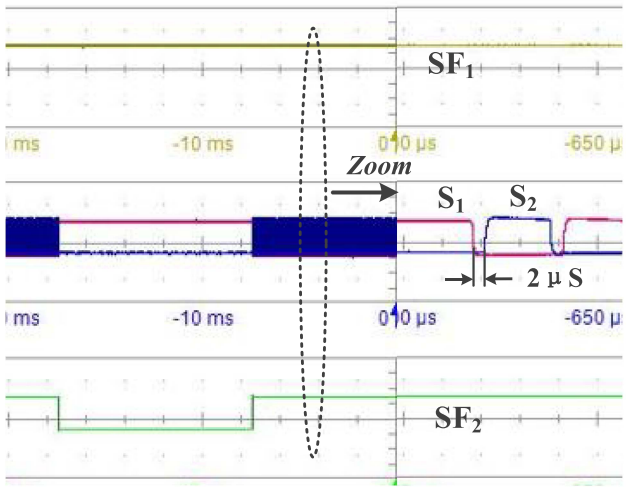

(a)

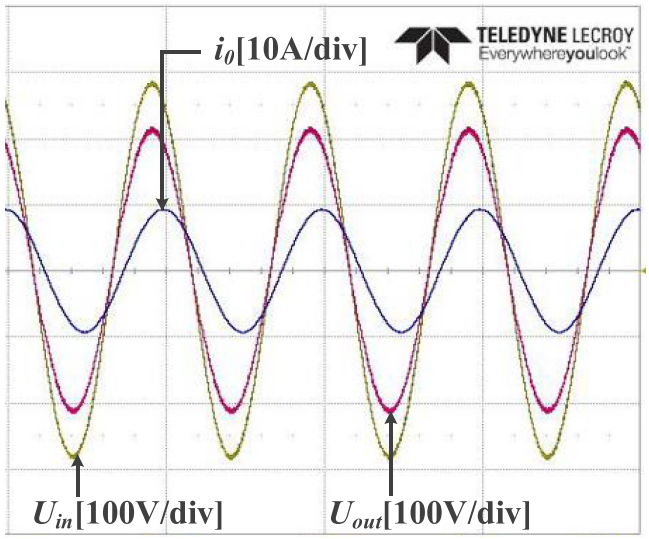

(b)

Fig. 15. Experimental waveformss of noninverting mode under resistive-inductive load ($U_{\text{in}} = 200$ Vrms, $U_{\text{out}} = 150$ Vrms, $R = 20\ \Omega$, and $L = 25$ mH).

the switches S_1 and S_2 and the input voltage are presented in Fig. 16(b). It can be seen that the peak voltage stress on switches S_1 and S_2 is equal to the input voltage.

Fig. 17 shows the waveforms of the converter under operating inverting mode when the load is resistive-inductive. Fig. 17(a) shows the waveforms of input voltage (U_{in}), output voltage (U_{out}), and output current (i_0). From Fig. 17(b), it appears that the peak voltage stress on capacitors C_1 and C_2 is equal to the input voltage, so there is no overvoltage problem. In addition, it can be seen that in the positive half cycle of the input voltage, the input capacitor C_{in} is connected in parallel with the absorption capacitor C_1, and in the negative half cycle, the input capacitor C_{in} is connected in parallel with the absorption capacitor C_2, capacitance symmetry is realized in each working process.

Fig. 18 shows the waveform of the experimental results when the converter output voltage is changed dynamically. It can be seen that the waveforms quality of the converter is good, which

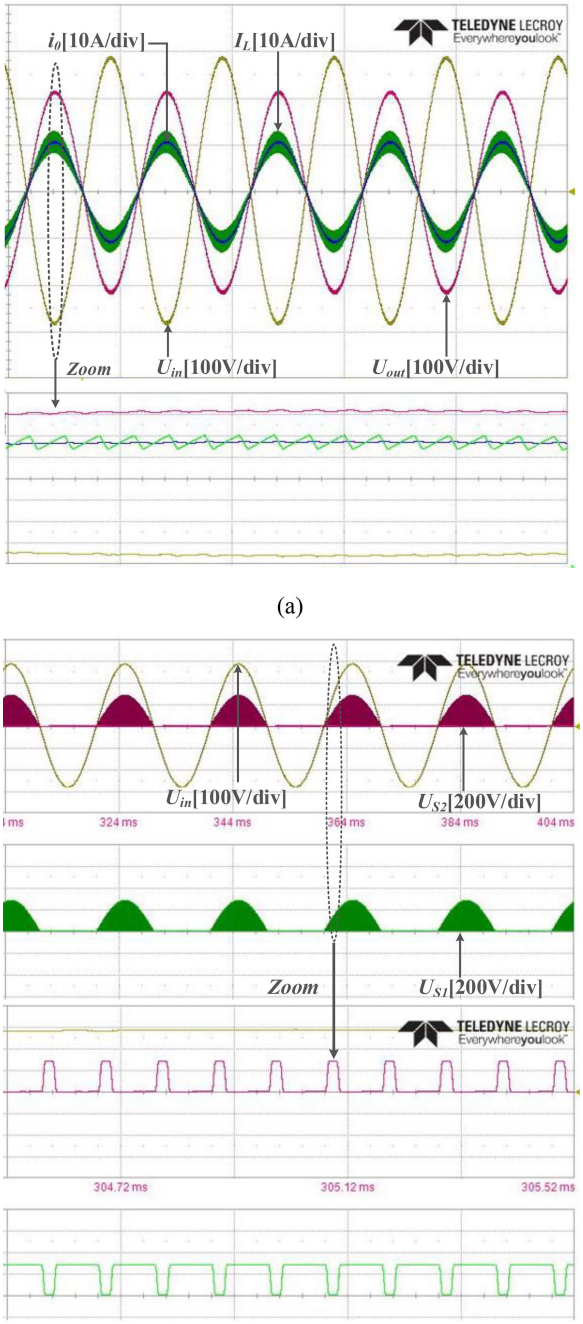

Fig. 16. Experimental waveformss of inverting mode under resistive load ($U_{\rm in}$ = 200 Vrms, $U_{\rm out}$ = 150 Vrms, and $R = 20\ \Omega$).

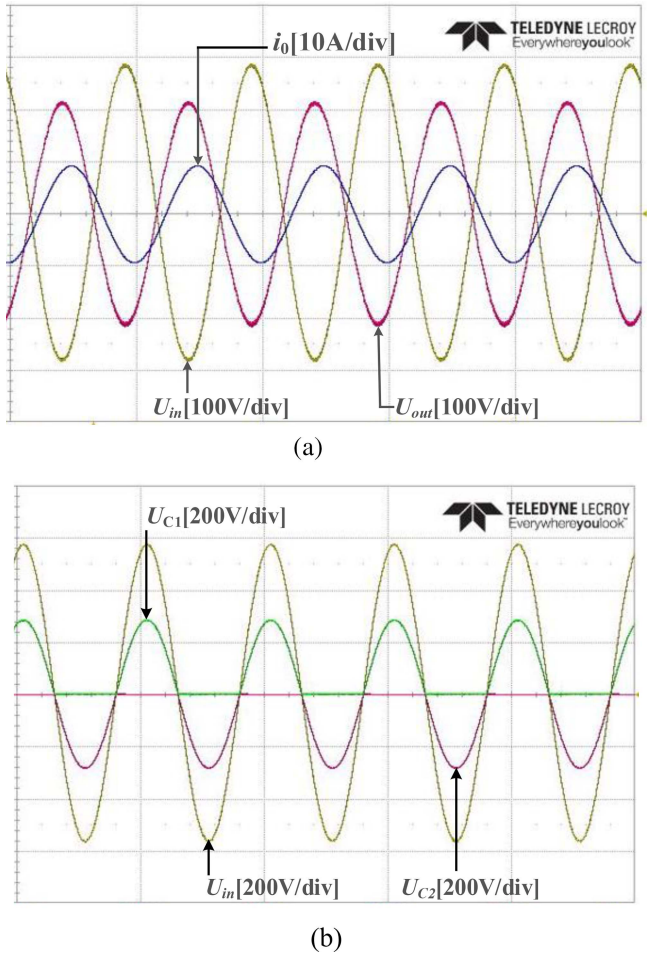

Fig. 17. Experimental waveformss of noninverting mode under resistive-inductive load ($U_{\rm in}$ = 200 Vrms, $U_{\rm out}$ = 150 Vrms, $R = 20\ \Omega$, $L = 25$ m).

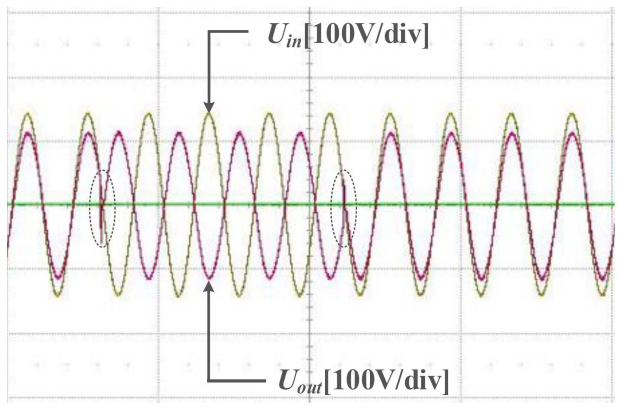

Fig. 18. Experimental waveforms of the converter switching between noninverting mode and inverting mode.

verifies that the converter has good dynamic performance and the converter has the ability to output bipolar voltage.

FLUKER MORMA 5000 POWER ANALYZER is used to analyze the efficiency of the converter under two working modes. The efficiency curve of the converter under different input voltages is shown in Fig. 19. The input voltage ranges from 80 to 180 Vrms, and the load includes pure resistive and resistive-inductive.

Under pure resistive load, the peak efficiency of the converter is 97.47%. Under resistive-inductive load, the peak efficiency of the converter is 96.36%. Consistent with the theoretical analysis, the efficiency of the proposed converter is significantly improved due to the reduction of the number of high-frequency operating switches.

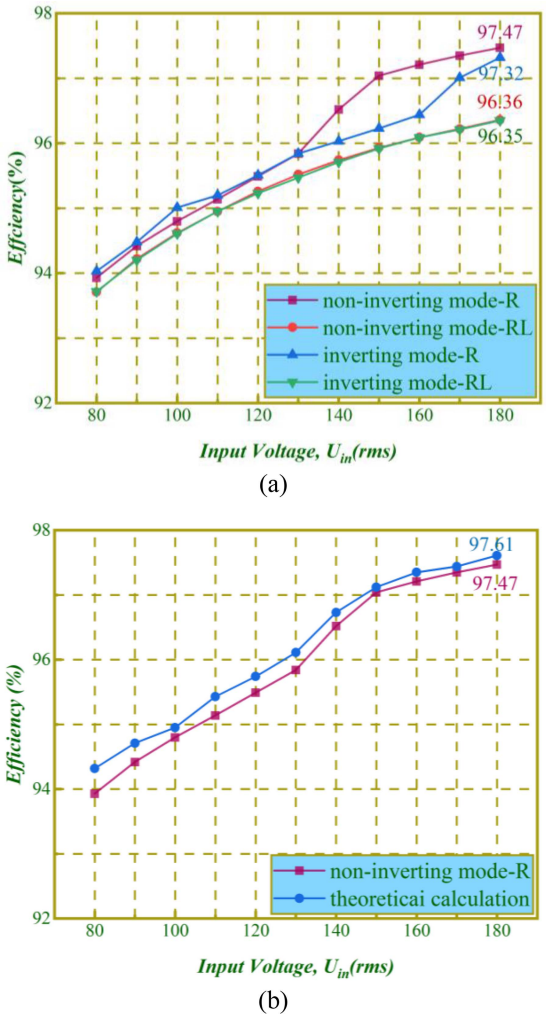

Fig. 19. Efficiency of the converter under two working modes. (a) Actual measured efficiency curve of converter. (b) Theoretical calculated and actual measured efficiency of converter.

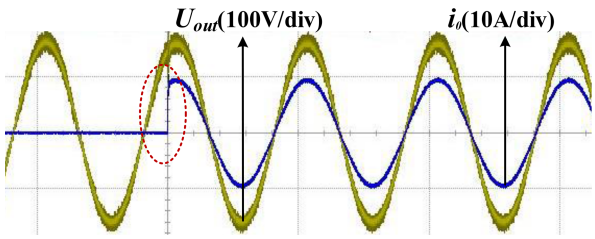

Fig. 20. Experimental results of loads change.

C. Transient Experimental Results of Proposed Converter

Fig. 20 shows experimental results of the converter when load changes from infinity to 20 Ω. At red dotted line mark in Fig. 20, load changes transiently, the output voltage U_{out} of converter does not change significantly, and output current i_0 changes rapidly from 0 to 7.5 A, indicating that converter has good transient response capability.

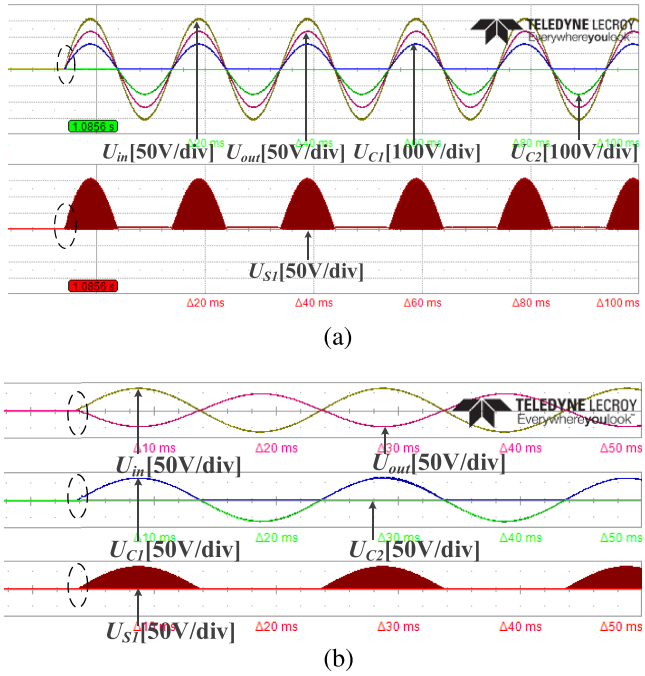

Fig. 21. Experiment results of the start-up precharge of the capacitors. (a) Noninverting mode. (b) Inverting mode.

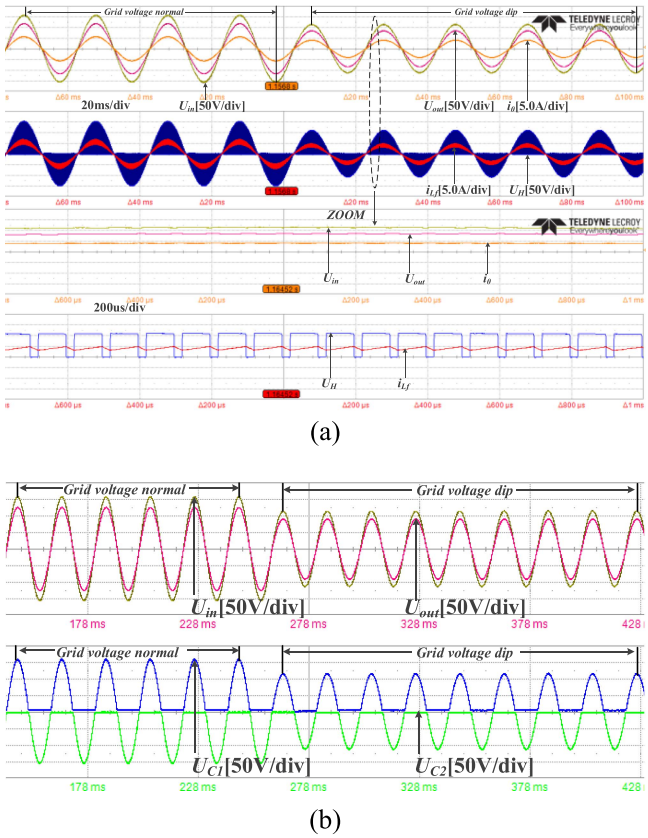

Fig. 22. Experimental results of the converter during grid voltage dip in the noninverting mode.

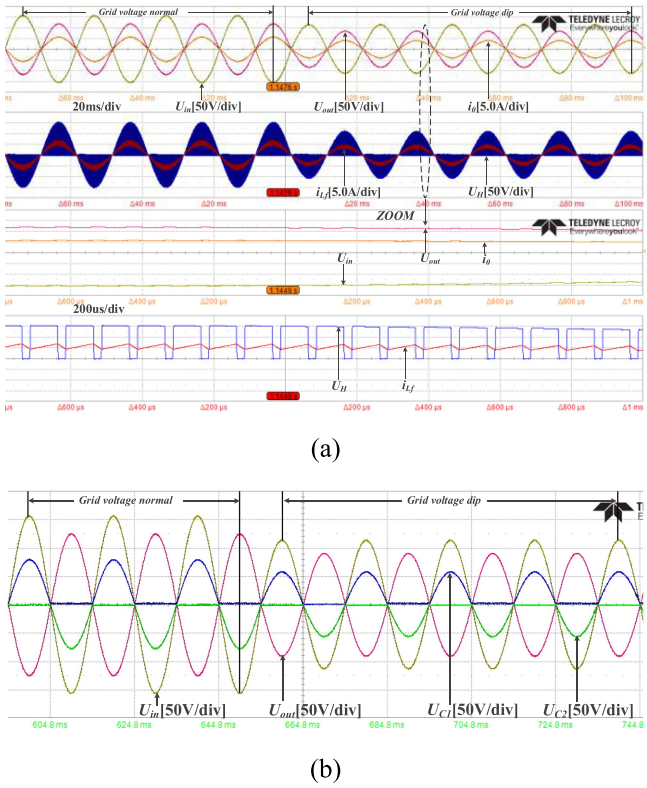

Fig. 23. Experimental results of the converter during grid voltage dip in the inverting mode.

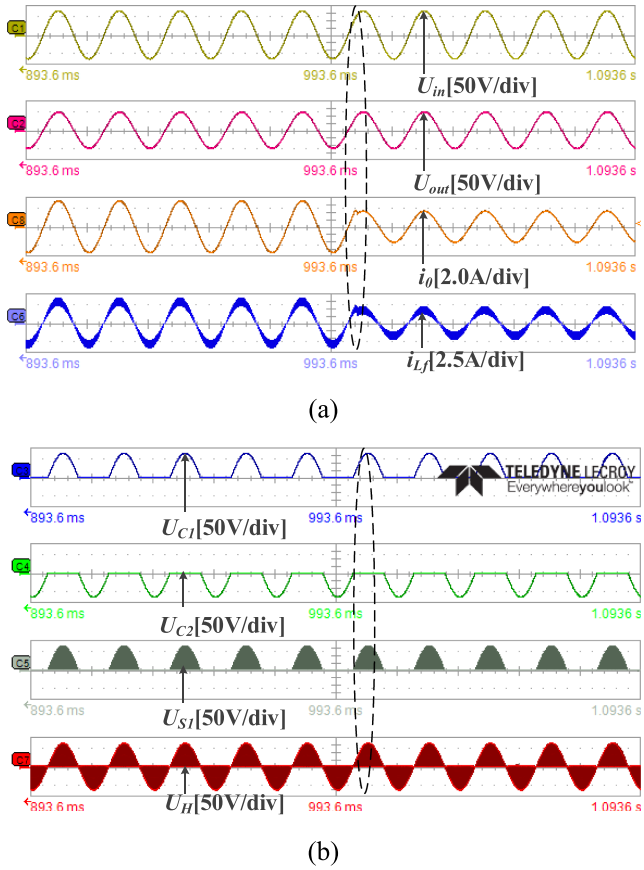

Fig. 24. Experimental results of the converter under pure resistive load step change in noninverting mode.

From Fig. 21, it can be seen that the voltages of capacitors C_1 and C_2 always follow the input ac voltage. When the input ac voltage gradually increases from 0 to the peak value in the positive half wave, the capacitor C_1 voltage also gradually increases from 0 to the peak value, and capacitor C_2 voltage is 0; When the input ac voltage gradually increases from 0 to the peak in the negative half wave, the capacitor C_2 voltage also increases from 0 to the peak at the negative half wave, and capacitor C_1 voltage is 0.

Fig. 22 shows the experimental results of the converter during grid voltage dip in the noninverting mode. From the experimental results, it can be seen that the converter can still operate normally when the voltage dip, and there are no abnormal conditions such as overvoltage or overcurrent. The inductance current i_{Lf} and voltage before output filtering U_H are still consistent with theoretical analysis.

From the experimental results shown in Fig. 23, it can be seen that the converter in the inverting mode can still operate normally when the grid voltage dip, and the converter has a good response to follow the grid voltage.

Fig. 24 shows the experimental results of the step change of pure resistive load. The load step changes from heavy load to light load at the dashed line in Fig. 5. During this process, the output current *i0* decreases, while the output voltage *U*out, capacitor voltage *UC1*, *UC2*, and switch *S1* voltage stress *US1* remain unchanged. Therefore, the experimental results can prove that the converter can work stably when the pure resistive load step change.

Fig. 25 shows the experimental results of the step change of resistive-inductive load. The load step changes from resistive-inductive load to pure resistive load at the dashed line in Fig. 6. From the experimental results, it can also be seen that when the resistive-inductive loads are dynamically step changed, the converter can also work stably.

From the experimental results in Fig. 26, it can be seen that the converter in inverting mode can operate stably when the resistive-inductive load step change.

D. The Proposed Converter Is Used for Dynamic Voltage Regulation

In order to understand the experimental conditions, the system equivalent wiring diagram of converter during voltage sag and swell test is shown in Fig. 27(a). U_{source} represents the source side voltage, U_{out} is converter output voltage, and U_{load} represents load voltage, in Fig. 27(a). Because the proposed direct ac–ac converter only changes the amplitude of ac voltage, the relationship between the three voltages (U_{source}, U_{out}, and U_{load}) in the system meets (26). Therefore, the proposed converter is very suitable for protecting voltage stability of sensitive loads, such as it can apply to dynamic voltage restorer (DVR) [33]. It should be noted that the standard voltage (or rated voltage) is defined as 110 Vrms due to the limitation of laboratory

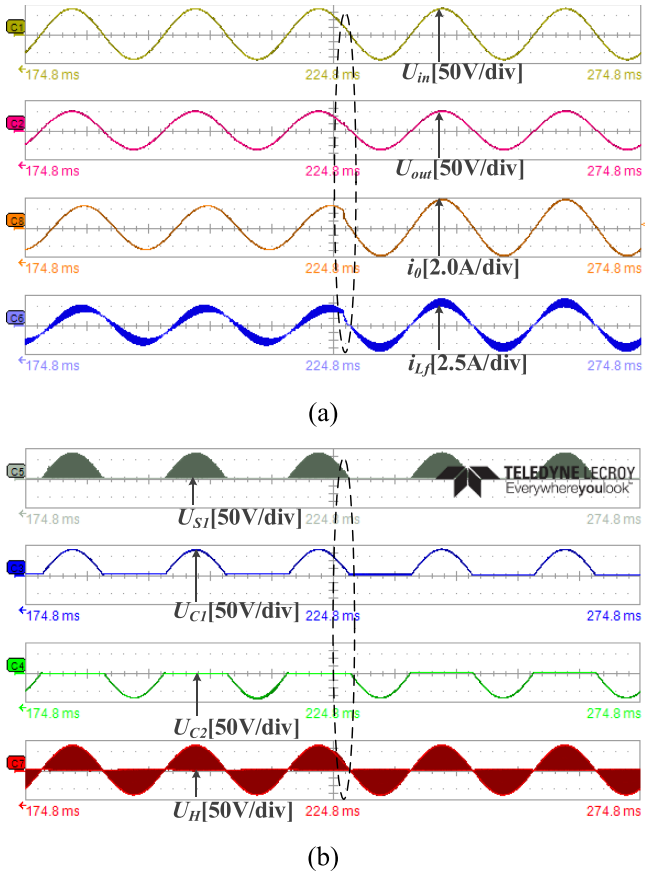

Fig. 25. Experimental results of the converter under resistive-inductive load step change in noninverting mode.

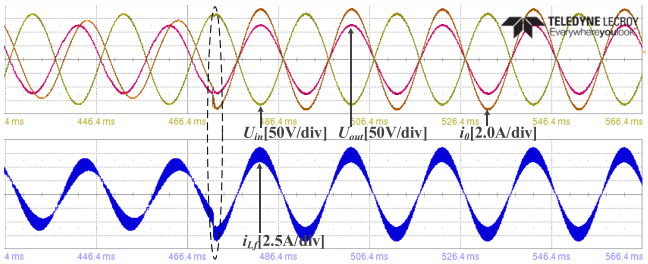

Fig. 26. Experimental results of the converter under resistive-inductive load step change in inverting mode.

equipment, the experimental results of voltage sag and swell are obtained under this condition

$$U_{\text{load}} = U_{\text{source}} + U_{\text{out}}. \tag{26}$$

Fig. 27(b)–(d) show experimental results of converter under source voltage transient conditions. From experimental results, it can be seen that converter is able to produce desired output voltage U_{out} regardless of voltage sag or voltage swell at the source side, so as to realize the compensation of the load side voltage and make the load always operate at the rated voltage conditions. Additionally, the experimental results show that the dynamic response of converter is fast, and phase-locked loop (PLL) is not needed in the experimental process. These

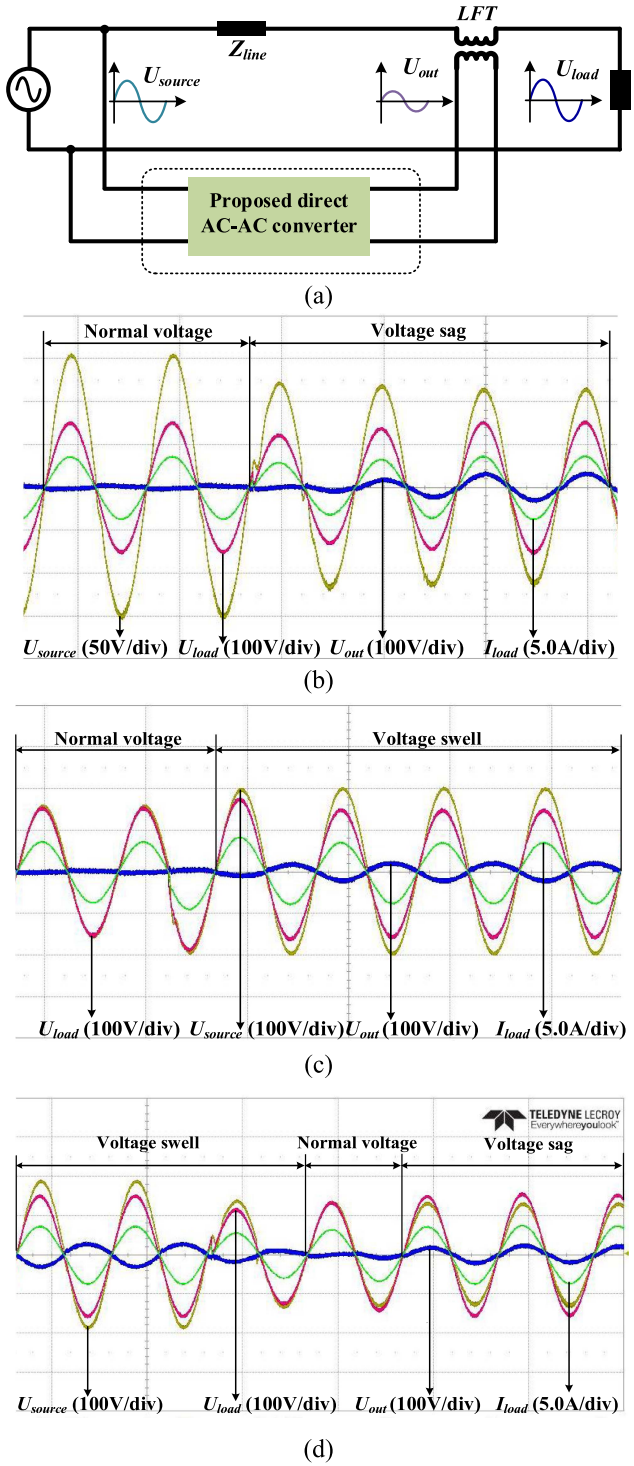

Fig. 27. Experimental result of converter under source voltage transient conditions. (a) System equivalent wiring diagram. (b) Source voltage sag. (c) Source voltage swell. (d) Source voltage sag and swell simultaneously.

characteristics of the proposed converter make it very suitable for ac voltage regulation field, especially in the application scenario where only the amplitude of ac voltage needs to be adjusted.

The experimental result in Fig. 28 is obtained under the condition that grid voltage with harmonics and load is resistive-inductive load. Comparing the experimental results in Figs. 28

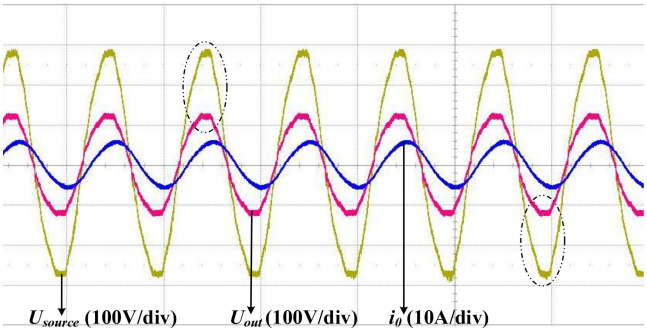

Fig. 28. Experimental results of grid voltage with harmonics.

and 27, it can be seen that the output voltage waveform quality will also deteriorate when the input voltage waveform quality of the converter becomes poor, which is consistent with the characteristics that the proposed direct ac–ac converter only changes ac voltage amplitude. Furthermore, it can be seen from experimental results that the load current waveform quality is less affected by grid voltage with harmonics.

VII. Conclusion

This article presents a single-phase reliable bipolar direct ac–ac converter consisting of two ac chopper legs with odd symmetry and a unipolar modulation strategy. The converter has the ability to output bipolar voltage gain, which makes it very suitable for addressing the problem of power grid voltage swell and sag. The converter has high reliability due to it overcomes the commutation problems. Thanks to the unipolar modulation strategy, the number switches working at high frequency in each operating mode are optimized, so the total switching losses can be effectively reduced in theory. Moreover, capacitor symmetry can be realized in the positive and negative half cycle of the input voltage. A detailed theoretical analysis including converters working process, design consideration and power losses calculation has been given, and validated by experimental results.

References

[1] F. C. L. Trindade, K. V. do Nascimento, and J. C. M. Vieira, "Investigation on voltage sags caused by DG anti-islanding protection," *IEEE Trans. Power Del.*, vol. 28, no. 2, pp. 972–980, Apr. 2013.

[2] J. Kaniewski, P. Szczesniak, M. Jarnut, and G. Benysek, "Hybrid voltage sag/swell compensators: A review of hybrid AC/AC converters," *IEEE Ind. Electron. Mag.*, vol. 9, no. 4, pp. 37–48, Dec. 2015.

[3] A. E. L. da Costa, C. B. Jacobina, N. Rocha, E. R. C. da Silva, and A. V. d. M. Lacerda Filho, "A single-phase AC–DC–AC unidirectional three-leg converter," *IEEE Trans. Ind. Electron.*, vol. 68, no. 5, pp. 3876–3886, May 2021.

[4] L. Yang, H. Zhao, S. Wang, and Y. Zhi, "Common-Mode EMI noise analysis and reduction for AC–DC–AC systems with paralleled power modules," *IEEE Trans. Power Electron.*, vol. 35, no. 7, pp. 6989–7000, Jul. 2020.

[5] T. Li, J. Chen, P. Cong, X. Dai, R. Qiu, and Z. Liu, "Online condition monitoring of DC-Link capacitor for AC/DC/AC PWM converter," *IEEE Trans. Power Electron.*, vol. 37, no. 1, pp. 865–878, Jan. 2022.

[6] A. Ebrahimian, S. Vahid, N. Weise, and A. EL-Refaie, "Two level AC-DC-AC converter design with a new approach to implement finite control set model predictive control," in *Proc. 22nd IEEE Int. Conf. Ind. Technol.*, 2021, pp. 514–520.

[7] Y. Sun, W. Xiong, M. Su, X. Li, H. Dan, and J. Yang, "Carrier-based modulation strategies for multimodular matrix converters," *IEEE Trans. Ind. Electron.*, vol. 63, no. 3, pp. 1350–1361, Mar. 2016.

[8] L. Qiu, L. Xu, K. Wang, Z. Zheng, and Y. Li, "Research on output voltage modulation of a five-level matrix converter," *IEEE Trans. Power Electron.*, vol. 32, no. 4, pp. 2568–2583, Apr. 2017.

[9] M. Vijayagopal, C. Silva, L. Empringham, and L. de Lillo, "Direct predictive current-error vector control for a direct matrix converter," *IEEE Trans. Power Electron.*, vol. 34, no. 2, pp. 1925–1935, Feb. 2019.

[10] S. Jayaprakasan, S. Ashok, and R. Ramchand, "Analysis of current error space phasor for a space vector modulated indirect matrix converter," *IEEE Trans. Ind. Electron.*, vol. 69, no. 6, pp. 5680–5689, Jun. 2022.

[11] G. H. P. Ooi, A. I. Maswood, and Z. Lim, "Five-level multiple-pole PWM AC–AC converters with reduced components count," *IEEE Trans. Ind. Electron.*, vol. 62, no. 8, pp. 4739–4748, Aug. 2015.

[12] K. Basu and N. Mohan, "A single-stage power electronic transformer for a three-phase PWM AC/AC drive with source-based commutation of leakage energy and common-mode voltage suppression," *IEEE Trans. Ind. Electron.*, vol. 61, no. 11, pp. 5881–5893, Nov. 2014.

[13] A. A. Khan, H. Cha, and H. Kim, "Magnetic integration of discrete-coupled inductors in single-phase direct PWM AC–AC converters," *IEEE Trans. Power Electron.*, vol. 31, no. 3, pp. 2129–2138, Mar. 2016.

[14] S. Sharifi, M. Monfared, and A. Nikbahar, "Highly efficient single-phase direct AC-to-AC converter with reduced semiconductor count," *IEEE Trans. Ind. Electron.*, vol. 68, no. 2, pp. 1130–1138, Feb. 2021.

[15] J.-H. Kim, B.-D. Min, B.-H. Kwon, and S.-C. Won, "A PWM buck-boost AC chopper solving the commutation problem," *IEEE Trans. Ind. Electron.*, vol. 45, no. 5, pp. 832–835, Oct. 1998.

[16] J. Hoyo, J. Alcala, and H. Calleja, "A high quality output AC/AC Cuk converter," in *Proc. IEEE 35th Annu. Power Electron. Specialists Conf.*, 2004, pp. 2888–2893.

[17] A. A. Khan, H. Cha, and H. F. Ahmed, "An improved single-phase direct PWM inverting buck–boost AC–AC converter," *IEEE Trans. Ind. Electron.*, vol. 63, no. 9, pp. 5384–5393, Sep. 2016.

[18] H. Shin, H. Cha, H. Kim, and D. Yoo, "Novel single-phase PWM AC–AC converters solving commutation problem using switching cell structure and coupled inductor," *IEEE Trans. Power Electron.*, vol. 30, no. 4, pp. 2137–2147, Apr. 2015.

[19] A. A. Khan, H. Cha, and H. Kim, "Magnetic integration of discrete-coupled inductors in single-phase direct PWM AC–AC converters," *IEEE Trans. Power Electron.*, vol. 31, no. 3, pp. 2129–2138, Mar. 2016.

[20] Y. Tang, C. Zhang, and S. Xie, "Z-Source AC-AC converters solving commutation problem," in *Proc. IEEE Power Electron. Specialists Conf.*, 2007, pp. 2672–2677.

[21] L. He, S. Duan, and F. Peng, "Safe-Commutation strategy for the novel family of quasi-z-source AC–AC converter," *IEEE Trans. Ind. Inform.*, vol. 9, no. 3, pp. 1538–1547, Aug. 2013.

[22] H. F. Ahmed, H. Cha, A. A. Khan, and H. Kim, "A family of high-frequency isolated single-phase Z-Source AC–AC converters with safe-commutation strategy," *IEEE Trans. Power Electron.*, vol. 31, no. 11, pp. 7522–7533, Nov. 2016.

[23] M.-K. Nguyen, Y.-G. Jung, and Y.-C. Lim, "Single-phase AC/AC converter based on quasi-Z-source topology," in *Proc. IEEE Int. Symp. Ind. Electron.*, 2009, pp. 261–265.

[24] M. Nguyen, Y. Lim, and Y. Kim, "A modified single-phase quasi-z-source AC–AC converter," *IEEE Trans. Power Electron.*, vol. 27, no. 1, pp. 201–210, Jan. 2012.

[25] L. He, J. Nai, and J. Zhang, "Single-Phase safe-commutation trans-z-source AC–AC converter with continuous input current," *IEEE Trans. Ind. Electron.*, vol. 65, no. 6, pp. 5135–5145, Jun. 2018.

[26] P. Li and Y. Hu, "Unified non-inverting and inverting PWM AC–AC converter with versatile modes of operation," *IEEE Trans. Ind. Electron.*, vol. 64, no. 2, pp. 1137–1147, Feb. 2017.

[27] H. F. Ahmed, H. Cha, A. A. Khan, and H. Kim, "A novel buck–boost AC–AC converter with both inverting and noninverting operations and without commutation problem," *IEEE Trans. Power Electron.*, vol. 31, no. 6, pp. 4241–4251, Jun. 2016.

[28] H. F. Ahmed, M. S. El Moursi, H. Cha, K. Al Hosani, and B. Zahawi, "A reliable single-phase bipolar buck–boost direct PWM AC–AC converter with continuous input/output currents," *IEEE Trans. Ind. Electron.*, vol. 67, no. 12, pp. 10253–10265, Dec. 2020.

[29] J. Kim and H. Cha, "Common-Ground-Structured high-reliability single-phase AC–AC converters," *IEEE Trans. Ind. Electron.*, vol. 70, no. 5, pp. 4672–4681, May 2023.
[30] H. F. Ahmed, M. S. E. Moursi, B. Zahawi, K. A. Hosani, and A. A. Khan, "Switching-Cell buck–boost AC–AC converter with common-ground and noninverting/inverting operations," *IEEE Trans. Power Electron.*, vol. 36, no. 12, pp. 13944–13957, Dec. 2021.
[31] C. Liu et al., "Novel bipolar-type direct AC–AC converter topology based on non-differential AC choppers," *IEEE Trans. Power Electron.*, vol. 34, no. 10, pp. 9585–9599, Oct. 2019.
[32] Y. Wang et al., "An improved bipolar-type AC–AC converter topology based on nondifferential dual-buck PWM AC choppers," *IEEE Trans. Power Electron.*, vol. 36, no. 4, pp. 4052–4065, Apr. 2021.
[33] S. Kim, H. -G. Kim, and H. Cha, "Dynamic voltage restorer using switching cell structured multilevel AC–AC converter," *IEEE Trans. Power Electron.*, vol. 32, no. 11, pp. 8406–8418, Nov. 2017.

Dongbo Guo received the B.S. and M.S. degrees in electrical engineering in 2016 and 2019, respectively, from Northeast Electric Power University, Jilin, China, where he is currently working toward the Ph.D. degree in electrical engineering.

In 2019, he was a Teaching Assistant with the School of Electrical Engineering, Northeast Electric Power University, Jilin, China. His current research interests include flexible operation and control of power grid based on ac/ac conversion, direct PWM ac/ac converters, and the application of high-power electronic conversion technology in smart grid.

Tianpeng Du was born in Heilongjiang Province, China, in 1998. He received the B.S. degree in electrical engineering from Harbin University of Science and Technology, Heilongjiang, China, in 2016. He is currently working toward the M.S. degree in electrical engineering with Northeast Electric Power University, Jilin, China.

His current research interests include high power density converter based on wide bandgap devices and direct PWM ac-ac converters.

Chuang Liu (Member, IEEE) received the M.S. degree from Northeast Electric Power University, Jilin, China, in 2009, and the Ph.D. degree from the Harbin Institute of Technology, Harbin, China, in 2013, both in electrical engineering.

From 2010 to 2012, he was with the Future Energy Electronics Center, Virginia Polytechnic Institute and State University, Blacksburg, VA, USA, as a Visiting Ph.D. Student, supported by the Chinese Scholarship Council. In 2013, he was an Associate Professor with the School of Electrical Engineering, Northeast Electric Power University, where since 2016, he has been a Professor. His research interests include power electronics based on ac and dc transformers for future hybrid ac–dc power grids, flexible operation and control of power grid based on acac transformation, and power-electronics-based power system stability analysis and control.

Pinjia Zhang (Senior Member, IEEE) received the B.Eng. degree in electrical engineering from Tsinghua University, Beijing, China, in 2006 and the master's and Ph.D. degrees in electrical engineering from Georgia Institute of Technology, Atlanta, GA, USA, in 2009 and 2010, respectively.

From 2010 to 2015, he was with the Electrical Machines Laboratory, GE Global Research Center, Niskayuna, NY, USA. Since 2015, he has been with the Department of Electrical Engineering, Tsinghua University, as an Associate Professor. He has authored or coauthored more than 80 papers in refereed journals and international conference proceedings, has more than 40 patent fillings in the U.S. and worldwide. His research interests include condition monitoring, diagnostics and prognostics techniques for electrical assets

Dr. Zhang was the recipient of IAS Andrew W. Smith Outstanding Young Member Achievement Award in 2018. He was also the recipient of three best paper awards from the IEEE IAS and IES society.

Zhongchen Pei was born in Liaoning Province, China, in 1994. He received the B.S. degree in electrical engineering from the Changchun Institute of Technology in Changchun, China, in 2017, and the M.S. degree in electrical engineering from the Changchun Institute of Technology, Changchun, China, in 2020. He is currently working toward the Ph.D. degree in electrical engineering with Northeast Electric Power University, Jilin, China.

His current research interests include hybrid distribution transformer, solid-state transformer, and hybrid MVdc/ac power grids.

Guanyu Yan received the M.S. degree in electrical engineering from Northeastern University, Liaoning, China, in 2014. He is currently working toward the Ph.D. in electrical engineering with Northeast Electric Power University, Jilin, China.

He was a Lecturer with the School of Electrical and Information Engineering, Beihua University, Jilin, China, in 2019. His current research interests include direct PWM ac/ac converters and hybrid transformer.

Guowei Cai received the B.S. and M.S. degrees in electrical engineering from Northeast Electric Power University, Jilin, China, in 1990 and 1993, respectively, and the Ph.D. degree from Harbin Institute of Technology, Harbin, China, in 1999.

He is currently a Professor of Electrical Engineering with Northeast Electric Power University. His research interests include power system stability analysis and control, and smart grid with renewable power generation.

Yibo Wang received the B.S., M.S. and Ph.D. degrees in electrical engineering from Northeast Electric Power University, Jilin, China, in 2010, 2016 and 2020, respectively.

His current research interests include renewable energy integration into power networks, power electronic equipment of power system, power quality, flexible regulation of distribution network, clean energy consumption, power market.

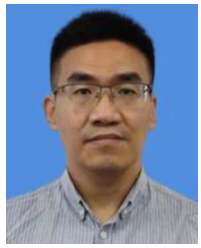

Rutian Wang received the M.S. degree from Northeast Electric Power University, Jilin, China, in 2005, and the Ph.D. degree from Harbin Institute of Technology, Harbin, China, in 2010, both in electrical engineering.

He is currently a Professor with the School of Electrical Engineering, Northeast Electric Power University. His research interests include the application of power electronic technology in power quality control and transmission and distribution system, the operation and control of new energy power generation system.